



## Suppression of Density Fluctuations in a Quantum Degenerate Fermi Gas

Christian Sanner, Edward J. Su, Aviv Keshet, Ralf Gommers, Yong-il Shin, Wujie Huang, and Wolfgang Ketterle

*MIT-Harvard Center for Ultracold Atoms, Research Laboratory of Electronics, and Department of Physics,  
Massachusetts Institute of Technology, Cambridge Massachusetts 02139, USA*

(Received 7 May 2010; published 19 July 2010)

We study density profiles of an ideal Fermi gas and observe Pauli suppression of density fluctuations (atom shot noise) for cold clouds deep in the quantum degenerate regime. Strong suppression is observed for probe volumes containing more than 10 000 atoms. Measuring the level of suppression provides sensitive thermometry at low temperatures. After this method of sensitive noise measurements has been validated with an ideal Fermi gas, it can now be applied to characterize phase transitions in strongly correlated many-body systems.

DOI: [10.1103/PhysRevLett.105.040402](https://doi.org/10.1103/PhysRevLett.105.040402)

PACS numbers: 03.75.Ss, 05.30.Fk, 67.85.Lm

Systems of fermions obey the Pauli exclusion principle. Processes that would require two fermions to occupy the same quantum state are suppressed. In recent years, several classic experiments have directly observed manifestations of Pauli suppression in Fermi gases. Antibunching and the suppression of noise correlations are a direct consequence of the forbidden double occupancy of a quantum state. Such experiments were carried out for electrons [1–3], neutral atoms [4,5], and neutrons [6]. In principle, such experiments can be done with fermions at any temperature, but in practice low temperatures increase the signal. A second class of (two-body) Pauli suppression effects, the suppression of collisions, requires a temperature low enough such that the de Broglie wavelength of the fermions becomes larger than the range of the interatomic potential and  $p$ -wave collisions freeze-out. Experiments observed the suppression of elastic collisions [7] and of clock shifts in radio frequency spectroscopy [8,9].

Here we report on the observation of Pauli suppression of density fluctuations. This is, like the suppression of collisions between different kinds of fermions [10], a many-body phenomenon which occurs only at even lower temperatures in the quantum degenerate regime, where the Fermi gas is cooled below the Fermi temperature and the low lying quantum states are occupied with probabilities close to 1. In contrast, an ideal Bose gas close to quantum degeneracy shows enhanced fluctuations [11].

The development of a technique to sensitively measure density fluctuations was motivated by the connection between density fluctuations and compressibility through the fluctuation-dissipation theorem. In this Letter, we validate our technique for determining the compressibility by applying it to the ideal Fermi gas. In future work, it could be extended to interesting many-body phases in optical lattices which are distinguished by their incompressibility [12]. These include the band insulator, Mott insulator, and also the antiferromagnet for which spin fluctuations, i.e., fluctuations of the difference in density between the two spin states are suppressed.

Until now, sub-Poissonian number fluctuations of ultracold atoms have been observed only for small clouds of bosons with typically a few hundred atoms [13–16] and directly [17,18] or indirectly [19] for the bosonic Mott insulator in optical lattices. For fermions in optical lattices, the crossover to an incompressible Mott insulator phase was inferred from the fraction of double occupations [20] or the cloud size [21]. Here we report the observation of density fluctuations in a large cloud of fermions, showing sub-Poissonian statistics for atom numbers in excess of 10 000 per probe volume.

The basic concept of the experiment is to repeatedly produce cold gas clouds and then count the number of atoms in a small probe volume within the extended cloud. Many iterations allow us to determine the average atom number  $N$  in the probe volume and its variance  $(\Delta N)^2$ . For independent particles, one expects Poisson statistics, i.e.,  $(\Delta N)^2/\langle N \rangle = 1$ . This is directly obtained from the fluctuation-dissipation theorem  $(\Delta N)^2/\langle N \rangle = nk_B T \kappa_T$ , where  $n$  is the density of the gas, and  $\kappa_T$  the isothermal compressibility. For an ideal classical gas  $\kappa_T = 1/(nk_B T)$ ,

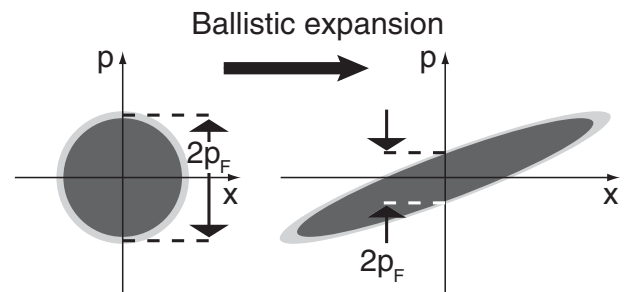


FIG. 1. Phase space diagram of ballistic expansion of a harmonically trapped Fermi gas. Ballistic expansion conserves phase space density and shears the initially occupied spherical area into an ellipse. In the center of the cloud, the local Fermi momentum and the sharpness of the Fermi distribution are scaled by the same factor, keeping the ratio of local temperature to Fermi energy constant. The same is true for all points in the expanded cloud relative to their corresponding unscaled in-trap points.

and one retrieves Poissonian statistics. For an ideal Fermi gas close to zero temperature with Fermi energy  $E_F$ ,  $\kappa_T = 3/(2nE_F)$ , and the variance  $(\Delta N)^2$  is suppressed below Poissonian fluctuations by the Pauli suppression factor  $3k_B T/(2E_F)$ . All number fluctuations are thermal, as indicated by the proportionality of  $(\Delta N)^2$  to the temperature in the fluctuation-dissipation theorem. Only for the ideal classical gas, where the compressibility diverges as  $1/T$ , one obtains Poissonian fluctuations even at zero temperature.

The counting of atoms in a probe volume can be done with trapped atoms, or after ballistic expansion. Ballistic expansion maintains the phase space density and therefore the occupation statistics. Consequently, density fluctuations are exactly rescaled in space by the ballistic expansion factors as shown in Fig. 1 [22,23]. Note that this rescaling is a unique property of the harmonic oscillator potential, so future work on density fluctuations in optical lattices must employ in-trap imaging. For the present work, we chose ballistic expansion. This choice increases the number of fully resolved bins due to optical resolution and depth of field, it allows adjusting the optimum optical density by choosing an appropriate expansion time, and it avoids image artifacts at high magnification.

We first present our main results, and then discuss important aspects of sample preparation, calibration of absorption cross section, data analysis and corrections for photon shot noise. Figure 2(a) shows an absorption image of an expanding cloud of fermionic atoms. The probe volume, in which the number of atoms is counted, is

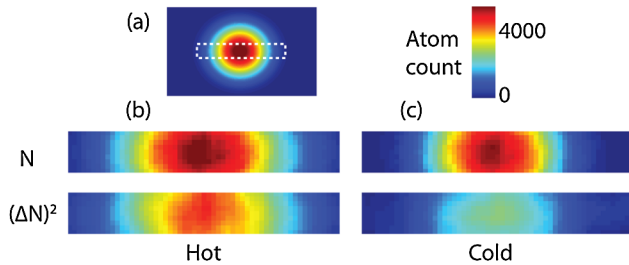


FIG. 2 (color online). Comparison of density images to variance images. For Poissonian fluctuations, the two images at a given temperature should be identical. The variance images were obtained by determining the local density fluctuations from a set of 85 images taken under identical conditions. (a) Two dimensional image of the optical density of an ideal Fermi gas after 7 ms of ballistic expansion. The noise data were taken by limiting the field of view to the dashed region of interest, allowing for faster image acquisition. (b) For the heated sample, variance and density pictures are almost identical, implying only modest deviation from Poissonian statistics. (c) Fermi suppression of density fluctuations deep in the quantum degenerate regime manifests itself through the difference between density and variance picture. Especially in the center of the cloud, there is a large suppression of density fluctuations. The variance images were smoothed over  $6 \times 6$  bins. The width of images (b) and (c) is 2 mm.

chosen to be 26  $\mu\text{m}$  in the transverse directions, and extends through the entire cloud in the direction of the line of sight. The large transverse size avoids averaging of fluctuations due to finite optical resolution. From 85 such images, after careful normalization [24], the variance in the measured atom number is determined as a function of position. After subtracting the photon shot noise contribution, a 2D image of the atom number variance  $(\Delta N)^2$  is obtained. For a Poissonian sample (with no suppression of fluctuations), this image would be identical to an absorption image showing the number of atoms per probe volume. This is close to the situation for the hottest cloud (the temperature was limited by the trap depth), whereas the colder clouds show a distinct suppression of the atom number variance, especially in the center of the cloud where the local  $T/T_F$  is smallest.

In Fig. 3, profiles of the variance are compared to theoretical predictions [25,26]. Density fluctuations at wave vector  $q$  are proportional to the structure factor  $S(q, T)$ . Since our probe volume (transverse size 26  $\mu\text{m}$ ) is much larger than the inverse Fermi wave vector of the expanded cloud ( $1/q_F = 1.1 \mu\text{m}$ ),  $S(q = 0, T)$  has been integrated along the line of sight for comparison with the experimental profiles. Within the local density approximation,  $S(q = 0, T)$  at a given position in the trap is the binomial variance  $n_k(1 - n_k)$  integrated over all momenta, where the occupation probability  $n_k(k, \mu, T)$  is obtained from the Fermi-Dirac distribution with a local chemical potential  $\mu$  determined by the shape of the trap. Figure 4 shows the dependence of the atom number variance on atom number for the hot and cold clouds. A statistical analysis of the data used in the figure is in [24].

The experiments were carried out with typically  $2.5 \times 10^6$   $^6\text{Li}$  atoms per spin state confined in a round crossed dipole trap with radial and axial trap frequencies  $\omega_r = 2\pi \times 160 \text{ s}^{-1}$  and  $\omega_z = 2\pi \times 230 \text{ s}^{-1}$  corresponding to an in-trap Fermi energy of  $E_F = k_B \times 2.15 \mu\text{K}$ . The sam-

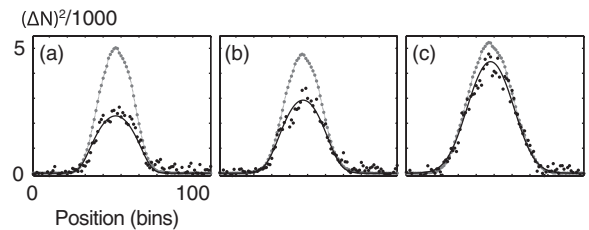


FIG. 3. Comparison of observed variances (black dots) with a theoretical model (black line) and the observed atom number (gray), at three different temperatures (a, b, and c), showing 50, 40, and 15% suppression. Noise thermometry is implemented by fitting the observed fluctuations, resulting in temperatures  $T/T_F$  of  $0.23 \pm .01$ ,  $0.33 \pm .02$ , and  $0.60 \pm .02$ . This is in good agreement with temperatures  $0.21 \pm .01$ ,  $0.31 \pm .01$ , and  $0.6 \pm .1$  obtained by fitting the shape of the expanded cloud [32]. The quoted uncertainties correspond to 1 standard deviation and are purely statistical.

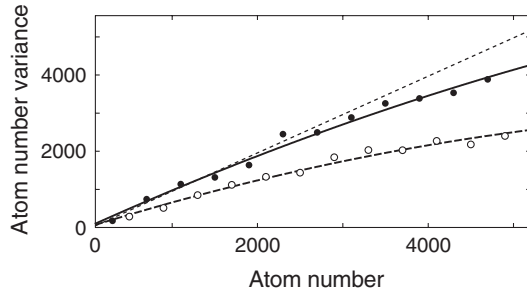


FIG. 4. Atom number variance vs average atom number. For each spatial position, the average atom number per bin and its variance were determined using 85 images. The filled and open circles in the figure are averages of different spatial bin positions with similar average atom number. For a hot cloud at  $T/T_F = 0.6$  (filled circles), the atom number variance is equal to the average atom number (dotted line, full Poissonian noise) in the spatial wings where the atom number is low. The deviation from the linear slope for a cold cloud at  $T/T_F = 0.21$  (open circles) is due to Pauli suppression of density fluctuations. There is also some suppression at the center of the hot cloud, where the atom number is high. The solid and dashed lines are quadratic fits for the hot and cold clouds to guide the eye.

ple was prepared by laser cooling followed by sympathetic cooling with  $^{23}\text{Na}$  in a magnetic trap.  $^6\text{Li}$  atoms in the highest hyperfine state were transferred into the optical trap, and an equal mixture of atoms in the lowest two hyperfine states was produced. The sample was then evaporatively cooled by lowering the optical trapping potential at a magnetic bias field  $B = 320 \pm 5$  G where a scattering length of  $-300$  Bohr radii ensured efficient evaporation. Finally, the magnetic field was increased to  $B = 520 \pm 5$  G, near the zero crossing of the scattering length. Absorption images were taken after 7 ms of ballistic expansion.

We were careful to prepare all samples with similar cloud sizes and central optical densities to ensure that they were imaged with the same effective cross section and resolution. Hotter clouds were prepared by heating the colder cloud using parametric modulation of the trapping potential. For the hottest cloud this was done near 520 G to avoid excessive evaporation losses.

Atomic shot noise dominates over photon shot noise only if each atom absorbs several photons. As a result, the absorption images were taken using the cycling transition to the lowest lying branch of the  $^2P_{3/2}$  manifold. However, the number of absorbed photons that could be tolerated was severely limited by the acceleration of the atoms by the photon recoil, which Doppler shifts the atoms out of resonance. Consequently, the effective absorption cross section depends on the probe laser intensity and duration. To remove the need for nonlinear normalization procedures, we chose a probe laser intensity corresponding to an average of only 6 absorbed photons per atom during a  $4 \mu\text{s}$  exposure. At this intensity, about 12% of the  $^6\text{Li}$  saturation intensity, the measured optical density was 20% lower than its low-intensity value [24]. For each

bin, the atom number variance  $(\Delta N)^2$  is obtained by subtracting the known photon shot noise from the variance in the optical density  $(\Delta\text{OD})^2$  [24]:

$$\frac{\sigma^2}{A^2} (\Delta N)^2 = (\Delta\text{OD})^2 - \frac{1}{\langle N_1 \rangle} - \frac{1}{\langle N_2 \rangle} \quad (1)$$

Here,  $\langle N_1 \rangle \langle N_2 \rangle$  are the average photon numbers per bin of area  $A$  in the image with (without) atoms and  $\sigma$  is the absorption cross section.

The absorption cross section is a crucial quantity in the conversion factor between the optical density and the number of detected atoms. For the cycling transition, the resonant absorption cross section is  $2.14 \times 10^{-13} \text{ m}^2$ . Applying the measured 20% reduction mentioned above leads to a value of  $1.71 \times 10^{-13} \text{ m}^2$ . This is an upper limit to the cross section due to imperfections in polarization and residual line broadening. An independent estimate of the effective cross section of  $1.48 \times 10^{-13} \text{ m}^2$  was obtained by comparing the integrated optical density to the number of fermions necessary to fill up the trap to the chemical potential. The value of the chemical potential was obtained from fits to the ballistic expansion pictures that allowed independent determination of the absolute temperature and the fugacity of the gas. We could not precisely assess the accuracy of this value of the cross section, since we did not fully characterize the effect of a weak residual magnetic field curvature on trapping and on the ballistic expansion. The most accurate value for the effective cross section was determined from the observed atom shot noise itself. The atom shot noise in the wings of the hottest cloud is Poissonian, and this condition determines the absorption cross section. Requiring that the slope of variance of the atom number  $(\Delta N)^2$  vs atom number  $N$  is unity (see Fig. 4) results in a value of  $(1.50 \pm 0.12) \times 10^{-13} \text{ m}^2$  for the effective cross section in good agreement with the two above estimates.

The spatial volume for the atom counting needs to be larger than the optical resolution. For smaller bin sizes (i.e., small counting volumes), the noise is reduced since the finite spatial resolution and depth of field blur the absorption signal. In our setup, the smallest bin size without blurring was determined by the depth of field, since the size of the expanded cloud was larger than the depth of field associated with the diffraction limit of our optical system. We determined the effective optical resolution by binning the absorption data over more and more pixels of the CCD camera, and determining the normalized central variance  $(\Delta N)^2/N$  vs bin size [24]. The normalized variance increased and saturated for bin sizes larger than  $26 \mu\text{m}$  (in the object plane), and this bin size was used in the data analysis. We observe the same suppression ratios for bin sizes as large as  $40 \mu\text{m}$ , corresponding to more than 10 000 atoms per bin.

For a cold fermion cloud, the zero temperature structure factor  $S(q)$  becomes unity for  $q > 2q_F$ . This reflects the

fact that momentum transfer above  $2q_F$  to any particle will not be Pauli suppressed by occupation of the final state. In principle, this can be observed by using bin sizes smaller than the Fermi wavelength, or by Fourier transforming the spatial noise images. For large values of  $q$ , Pauli suppression of density fluctuations should disappear, and the noise should be Poissonian. However, our imaging system loses its contrast before  $q \approx 2q_F$  [24].

Observation of density fluctuations, through the fluctuation-dissipation theorem, determines the product of temperature and compressibility. It provides an absolute thermometer, as demonstrated in Fig. 3 if the compressibility is known or is experimentally determined from the shape of the density profile of the trapped cloud [17,27]. Because variance is proportional to temperature for  $T \ll T_F$ , noise thermometry maintains its sensitivity at very low temperature, in contrast to the standard technique of fitting spatial profiles.

Density fluctuations lead to Rayleigh scattering of light. The differential cross section for scattering light of wave vector  $k$  by an angle  $\theta$  is proportional to the structure factor  $S(q)$ , where  $q = 2k \sin(\theta/2)$  [26]. In this work, we have directly observed the Pauli suppression of density fluctuations and therefore  $S(q) < 1$ , implying suppression of light scattering at small angles (corresponding to values of  $q$  inversely proportional to our bin size). How are the absorption images affected by this suppression? Since the photon recoil was larger than the Fermi momentum of the expanded cloud, large-angle light scattering is not suppressed. For the parameters of our experiment, we estimate that the absorption cross section at the center of a  $T = 0$  Fermi cloud is reduced by only 0.3% due to Pauli blocking [28]. Although we have not directly observed Pauli suppression of light scattering, which has been discussed for over 20 years [28–30], by observing reduced density fluctuations we have seen the underlying mechanism for suppression of light scattering.

In conclusion, we have established a sensitive technique for determining atomic shot noise and observed the suppression of density fluctuations in a quantum degenerate ideal Fermi gas. This technique is promising for thermometry of strongly correlated many-body systems and for observing phase-transitions or cross-overs to incompressible quantum phases.

We acknowledge Joseph Thywissen and Markus Greiner for useful discussions. This work was supported by NSF and the Office of Naval Research, AFOSR (through the MURI program), and under Army Research Office grant no. W911NF-07-1-0493 with funds from the DARPA Optical Lattice Emulator program.

*Note added in proof.*—Results similar to ours are reported in Ref. [31].

- [1] W. D. Oliver, J. Kim, R. C. Liu, and Y. Yamamoto, *Science* **284**, 299 (1999).
- [2] M. Henny *et al.*, *Science* **284**, 296 (1999).
- [3] H. Kiesel, A. Renz, and F. Hasselbach, *Nature (London)* **418**, 392 (2002).
- [4] T. Rom *et al.*, *Nature (London)* **444**, 733 (2006).
- [5] T. Jelte *et al.*, *Nature (London)* **445**, 402 (2007).
- [6] M. Iannuzzi *et al.*, *Phys. Rev. Lett.* **96**, 080402 (2006).
- [7] B. DeMarco *et al.*, *Phys. Rev. Lett.* **82**, 4208 (1999).
- [8] M. W. Zwierlein, Z. Hadzibabic, S. Gupta, and W. Ketterle, *Phys. Rev. Lett.* **91**, 250404 (2003).
- [9] S. Gupta *et al.*, *Science* **300**, 1723 (2003).
- [10] B. DeMarco, S. B. Papp, and D. S. Jin, *Phys. Rev. Lett.* **86**, 5409 (2001).
- [11] J. Estève *et al.*, *Phys. Rev. Lett.* **96**, 130403 (2006).
- [12] Q. Zhou, Y. Kato, N. Kawashima, and N. Trivedi, *arXiv:0901.0606*.
- [13] C. S. Chuu *et al.*, *Phys. Rev. Lett.* **95**, 260403 (2005).
- [14] J. Estève *et al.*, *Nature (London)* **455**, 1216 (2008).
- [15] S. Whitlock, C. F. Ockeloen, and R. J. C. Spreeuw, *Phys. Rev. Lett.* **104**, 120402 (2010).
- [16] A. Itah *et al.*, *Phys. Rev. Lett.* **104**, 113001 (2010).
- [17] N. Gemelke, X. Zhang, C. L. Hung, and C. Chin, *Nature (London)* **460**, 995 (2009).
- [18] M. Greiner (unpublished).
- [19] M. Greiner, O. Mandel, T. W. Hänsch, and I. Bloch, *Nature (London)* **419**, 51 (2002).
- [20] R. Jördens *et al.*, *Nature (London)* **455**, 204 (2008).
- [21] U. Schneider *et al.*, *Science* **322**, 1520 (2008).
- [22] S. Gupta, Z. Hadzibabic, J. R. Anglin, and W. Ketterle, *Phys. Rev. Lett.* **92**, 100401 (2004).
- [23] G. M. Bruun and C. W. Clark, *Phys. Rev. A* **61**, 061601(R) (2000).
- [24] See supplementary material at <http://link.aps.org/supplemental/10.1103/PhysRevLett.105.040402> for additional details.
- [25] Y. Castin, in *Proceedings of the International School of Physics Enrico Fermi, Course CLXIV*, edited by M. Inguscio, W. Ketterle, and C. Salomon (IOS, Amsterdam, 2008).
- [26] D. Pines and P. Nozières, *The Theory of Quantum Liquids* (Addison-Wesley, MA, 1988), Vol. 1.
- [27] Q. Zhou and T. L. Ho, *arXiv:0908.3015*.
- [28] A. Görlitz, A. P. Chikkatur, and W. Ketterle, *Phys. Rev. A* **63**, 041601(R) (2001).
- [29] K. Helmerson, M. Xiao, and D. E. Pritchard, in *International Quantum Electronics Conference 1990, Book of Abstracts*, econf QTHH4 (1990).
- [30] B. Shuve and J. H. Thywissen, *J. Phys. B* **43**, 015301 (2010). (and references therein)
- [31] T. Mueller *et al.*, *Phys. Rev. Lett.* **105**, 040401 (2010).
- [32] W. Ketterle and M. W. Zwierlein, in *Proceedings of the International School of Physics Enrico Fermi, Course CLXIV*, edited by M. Inguscio, W. Ketterle, and C. Salomon (IOS, Amsterdam, 2008).